Compaction of quartz sands by pressure solution using a Cole-Cole distribution of relaxation times

A. Revil,[1] P. Leroy,[1] A. Ghorbani,[2] N. Florsch,[2] and A. R. Niemeijer[3]

[1] Stressed water-infiltrated silica rocks may deform by pervasive pressure solution transfer (PPST), which involves dissolution of the grain-to-grain contacts, transport by diffusion of the solute, and precipitation on the free surfaces of the grains. A fundamental question regarding this process is how to model rheological behavior at stresses and temperatures typical of the crust of the Earth. A Voigt-type poroviscoplastic model is modified by using a Cole-Cole distribution of relaxation times rather than a Dirac distribution used previously. The motivation of this choice is to account for the distribution of the grain size in the compaction of the porous aggregate assuming that this distribution obeys approximately a log normal distribution. This grain size distribution depends upon the initial grain size distribution and cataclasis in the early stage of compaction. We compared this modified viscoplastic model with the full set of experimental data obtained in various conditions of mean grain size, effective stress, and temperature by Niemeijer et al. (2002). These data provide tests of all aspects of the model, which can be considered to have no free parameters. We show the experiments of Niemeijer et al. (2002) on PPST are primarily diffusion-limited. The grain size distributions observed for three samples imply that the distribution of the relaxation time covers 5 orders of magnitude in grain size.

1. Introduction

[2] Pervasive pressure solution transfer (PPST) describes the irreversible compactional process of mass transfer in rocks in response to stress and temperature fluctuations [e.g., *Rutter*, 1976, 1983; *Niemeijer and Spiers*, 2002; *Skvortsova*, 2004, and references therein]. Other mechanism of deformation are possible like those associated with microcracking [*Karner et al.*, 2003]. PPST is associated with stress concentration at grain-to-grain contacts increasing solubility of the solid in the pore fluid, diffusion of the solute along grain-to-grain contacts, and precipitation on free faces of the grains. The understanding of PPST can lead to the understanding of locking/unlocking processes that affect granular gouge of active faults during the tectonic cycle (see recent papers by *Montési* [2004] and *Yasuhara et al.* [2005]) and compaction of quartz sands in sedimentary basins [e.g., *Wahab*, 1998]. In addition, PPST could explain soft creep rheology observed in the brittle-ductile transition zone of the crust and within the seismogenic crust itself [*Ivins*, 1996].

[3] For quartz sands, several research scientists have modeled pressure solution using a Newtonian viscous law [e.g., *Rutter*, 1976, 1983; *Dewers and Hajash*, 1995; *Renard et al.*, 1997; *Yang*, 2000; *He et al.*, 2002, 2003]. In contrast, *Stephenson et al.* [1992] described the occurrence of PPST of quartz sands in sedimentary basins, over long periods of time, as being a purely plastic compaction. *Revil* [1999] proposed a unified model, which takes the form of a poroviscoplastic (Voigt-type) linear model with a single relaxation time associated with the mean grain size of the porous medium (Figure 1). The microscopic reasons for this behavior were explored by *Revil* [2001], who proposed the existence of a stress threshold at the grain-to-grain contact below which PPST stops. Additional evidences in favor of this model were recently presented by *Yasuhara et al.* [2003, 2004, 2005] and *Alcantar et al.* [2003]. Implications of this model for travelling solitary waves were explored by *Yang* [2002]. However, there is the need to test further the validity of the model for a wide range of mean grain sizes, temperature, and effective stresses and to incorporate in this model a wider grain size distribution than just using a single value for the grain size.

[4] In section 2, the model of *Revil* [1999] is modified to account for the distribution of grain size in the rheological model. To reach this goal, we use a Cole-Cole distribution of relaxation times (rather than a single value) in the viscoplastic response of the porous aggregate. This is equivalent to assuming that the grain size distribution obeys a log normal distribution. The model of *Revil* [1999] is also modified to

[1]Department of Hydrogeophysics and Porous Media, CNRS-CEREGE, University Paul Cézanne-Aix-Marseille III, Aix-en-Provence, France.
[2]Department of Applied Geophysics, University Paris VI, Paris, France.
[3]High Pressure and Temperature Laboratory, Faculty of Geosciences, Utrecht University, Utrecht, Netherlands.
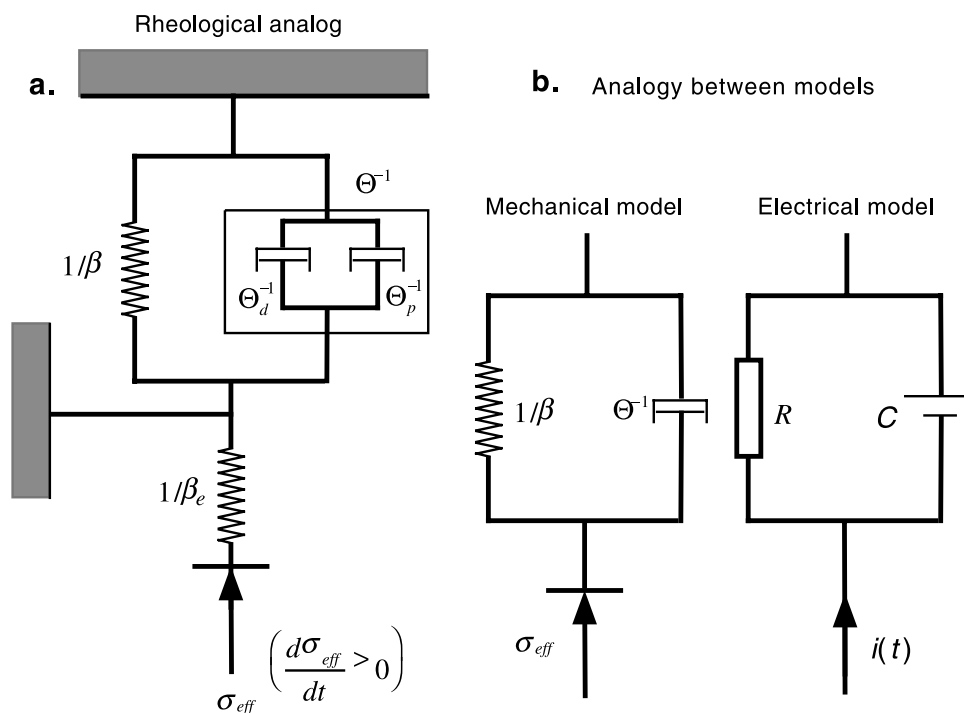
Figure 1. Sketch of the compactional model. (a) The deformation of a representative elementary volume of quartz sand follows a linear poroviscoplastic (Voigt-type) rheological behavior. The springs in parallel with the dashpot represent the plastic (thermostatic) equilibrium state, whereas the dashpots represent the kinetics of PPST at the grain-to-grain contacts (the dashpots "p" and "d" correspond to dissolution/ precipitation chemistry and diffusion-limited processes, respectively) (modified from *Revil* [2001]). An additional spring models the poroelastic response of the medium. (b) Analogy between a Voigt-type viscoplastic model (a dashpot in parallel with an anelastic spring) and an electrical circuit in which a resistor (R is the resistance) is in parallel with a capacitor (C is the capacitance). Such an electrical model is classically used to model the induced polarization response of water-saturated porous rocks.

account for the nonlinear behavior of the deformation/ effective stress constitutive law observed at high effective stresses (section 3). Despite the fact that this modification changes the results little at effective stress conditions prevailing in the upper crust of the Earth, it seems to us important to extend our model to a wide range of T-P conditions. In section 4, a nonlinear optimization scheme based on the Simplex algorithm is used to compare the compactional model to all the experimental data of *Niemeijer et al.* [2002]. *Niemeijer et al.* [2002] presented a unique series of experimental data in which they investigated the influence of temperature (in the range 400–600°C), effective stress (in the range 50–150 MPa), and mean grain size (10–86 μm) upon the compactional response of several quartz aggregates. In addition, the grain size distributions resulting from the compaction process and cataclasis was measured by *Niemeijer et al.* [2002] for three samples, spanning over 2 orders of magnitude in grain size. Consequently, these data offer a unique opportunity to test our compaction model.

[5] Five predictions made by our model are tested for the first time in this paper: (1) The plastic limit of the compactional response of the porous aggregate is independent of the mean grain size of the aggregate. (2) The temperature dependence of the (long-term or plastic) compaction coefficient can be determined using an Arrhenius law. (3) The mean relaxation time of the viscoplastic model can be

described (within a factor 2) using the mean grain diameter of the aggregate and temperature. (4) The relaxation time distribution (RTD) can be directly related to the particle size distribution (PSD) assuming a log normal distribution for the latter; the model should be flexible enough to incorporate other PSDs. (5) The same compactional model can be used to explain the full range of data obtained by *Niemeijer et al.* [2002] including the short-term viscous behavior and the long-term plastic limit.

2. Theoretical Background

2.1. Debye Distribution of Relaxation Times

[6] We make the following assumptions: (1) the rock is an isotropic granular material, (2) the mineral of the granular aggregate is silica, and (3) in this section the grain size

Table 1. Temperature Dependence of Model Parameters[a]

Parameter	Temperature Dependence $\wp = \wp_0 \exp(-E_\wp/RT)$	
Solubility	$C_0 = 67.6$ kg m^{-3} (1)	$E_C = 21.7$ kJ mol^{-1} (1)
Diffusivity	$D_0 = 5.2 \times 10^{-8}$ m^2 s^{-1} (2)	$E_D = 13.5$ kJ mol^{-1} (2)
Rate constant	$k_+^0 = 31.3$ mol m^{-2} s^{-1} (3)	$E_k = 71.3$ kJ mol^{-1} (3)
Compressibility	$\beta_0 = 2.6 \times 10^{-8}$ Pa^{-1} (4)	$E_\beta = 17$ kJ mol^{-1}(4)

[a]Notes: 1, *Iler* [1979]; 2, *Revil* [2001]; note for comparison, *Dewers and Ortoleva* [1990] used $D_0 \sim 1 \times 10^{-8}$ m^2 s^{-1} and $E_D = 40$ kJ mol^{-1} while *Nakashima* [1995] used $E_D = 15$ kJ mol^{-1}; 3, *Dove and Crerar* [1990]; 4 this work.
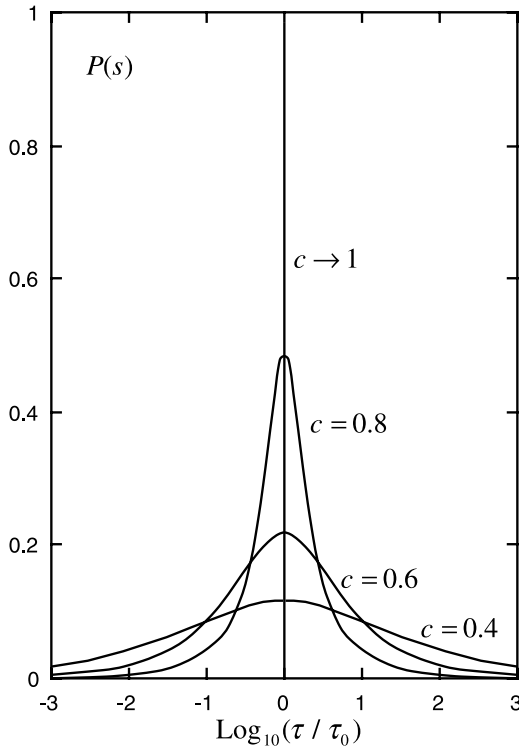
Figure 2. Distribution of relaxation times $P(s)$ where $s \equiv \ln(\tau/\tau_0)$ for various values of the Cole-Cole exponent c. Note that smaller values of the exponent corresponds to broader distributions of relaxation times. The case $c = 1$ yields a Dirac distribution. The case $0.5 \leq c \leq 1$ is very similar to a Gaussian distribution. For $c < 0.5$, the Cole-Cole distribution has a longer tail than the Gaussian distribution.

distribution obeys a delta (Dirac) distribution with d_0 the mean grain size. Under these assumptions and neglecting mechanical deformation (grain rearrangement [e.g., *Revil et al.*, 2002]), the compactional response of the porous aggregate is described by the following linear constitutive law [*Revil*, 1999]:

$$\tilde{\phi}(t) = \beta(t) \otimes \frac{d\sigma_{eff}(t)}{dt} + \sigma_{eff}(t) \otimes \frac{d\beta(t)}{dt}, \tag{1}$$

$$\tilde{\phi}(t) \equiv (\phi_0 - \phi(t))/\phi_0, \tag{2}$$

$$\beta(t) \equiv \beta[1 - \exp(-t/\tau_0)], \tag{3}$$

where circled cross stands for the Stieltjes convolution product. In equations (1)–(3), t is time, $\beta(t)$ is the time-dependent compressibility of the porous aggregate, β is its long-term plastic compressibility (compaction coefficient), τ_0 is the relaxation time, $\sigma_{eff} = \sigma - p$ is the effective stress, σ is the confining pressure, p the pore fluid pressure, $\phi(t)$ is porosity at time t, and ϕ_0 is the initial porosity at the beginning of the PPST process. The origin of time coincides with the instant at which the material, in a relaxed reference state, is subjected to the application of effective stress. The

porosity ϕ_0 is the porosity following the application of the stress. So that the initial poroelastic compaction represents the starting reference state; initial poroelastic compaction is investigated in Appendix A. This elastic compaction process follows instantaneously the stress variations and is reversible.

[7] The rock behavior is modeled to have memory of the highest effective stress experienced by the grain-to-grain contact during its history because of the increase of the grain-to-grain contiguity associated with the compaction. The previous compactional response holds as long as

$$d\sigma_{eff}/dt \geq 0. \tag{4}$$

When the effective stress decreases, the deformation response follows essentially a poroelastic behavior corresponding to the relaxation of the elastic energy stored in the sample.

[8] The relaxation time in equation (3) is given by (Figure 1a),

$$\tau_0 = \beta/\Theta, \tag{5}$$

$$\Theta^{-1} = \Theta_d^{-1} + \Theta_p^{-1}, \tag{6}$$

$$\Theta_d = \left(\frac{32\Omega}{k_b T}\right) \frac{C\omega D}{\rho_g d_0^3}, \tag{7}$$

$$\Theta_p = \left(\frac{3\Omega^2}{k_b T N}\right) \frac{k_+}{d_0}, \tag{8}$$

where T is the temperature (in K), C (in kg m^{-3}) is the solubility of the grain surface in the pore water solution in equilibrium with quartz at fluid pressure and temperature, ω is the effective thickness of the diffusion pathways at the grain-to-grain contacts ($\sim$2 nm, see discussions by *Revil* [2001]), D (in m^2 s^{-1}) is the diffusivity of silica at the grain-to-grain contacts, d_0 (in m) is the grain diameter, Ω is the molecular volume of silica (3.77×10^{-29} m^3), k_+ is the dissolution rate constant, k_b is the Boltzmann constant (1.381×10^{-23} J K^{-1}), ρ_g is the density of the grains, and N is Avogadro's number (6.02×10^{23} mol^{-1}). The numerical constants entering equations (7) and (8) and the temperature dependence of the various parameters involved in these equations are reported in Table 1.

[9] *Revil* [2001] showed that diffusion of the solute at the grain-to-grain contacts is one or 2 orders of magnitude smaller than that in the bulk pore water. This was recently confirmed by laboratory experiments [e.g., *Alcantar et al.*, 2003; *Yasuhara et al.*, 2003, 2004]. In low-porosity shales and in compacted bentonites (both having small pore sizes), *Revil et al.* [2005] and *Leroy et al.* [2006] reached similar conclusions based on modeling of coupling phenomena that affects diffusion of ionic species in charged media.

[10] The model of *Revil* [1999] corresponds to a Voigt-type linear viscoplastic model represented by a dashpot in parallel with an anelastic spring. From the perspective of the differential equation governing the system, the behavior is analogous to an electrical circuit formed by a resistor in
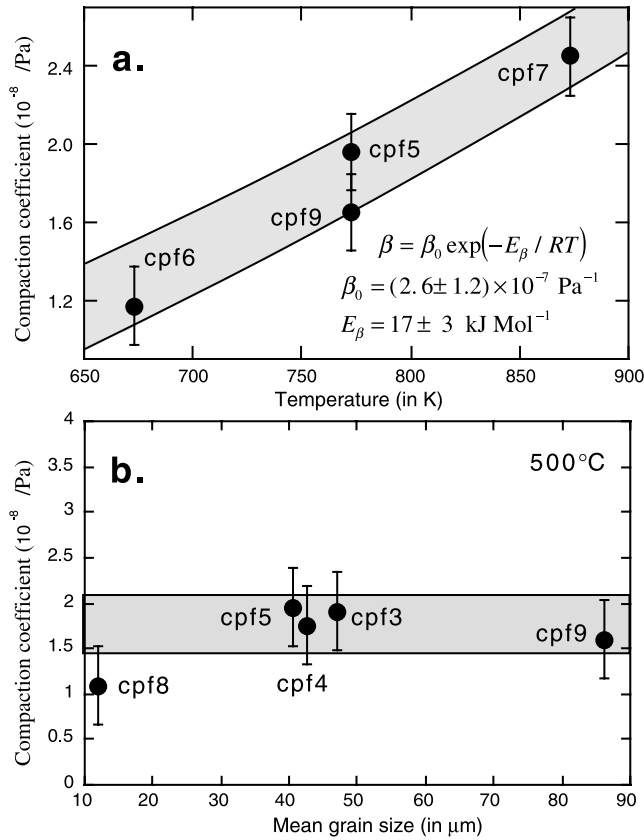
Figure 3. Long-term compaction coefficient β is determined using the plastic equilibrium compactional response of the aggregates and optimization of the model parameters. The solid circles correspond to the data from *Niemeijer et al.* [2002] (all runs). (a) The temperature dependence of the compaction coefficient can be described using an Arrhenius's law. (b) The compaction coefficient does not depend on the mean grain size. The thickness of the grey band represents the uncertainty in the determination of the compaction coefficient.

parallel with a capacitor (Figure 1b). In this case, the relaxation time is given by a Dirac (delta) distribution and takes the discrete value τ_0. In the study of the induced polarization of porous materials, this is known as a Debye relaxation or distribution.

2.2. Cole-Cole Distribution of the Relaxation Times

[11] When the grain size distribution cannot be described by a unique value, the relaxation time distribution (RTD) exhibited by the compactional response of a porous aggregate cannot be described by a single value of the relaxation time, hence by a Dirac distribution. If the effective stress variation follows a Heaviside (step) distribution, grain crushing associated with cataclasis in the first stage of deformation, increases the distribution of the grain size [e.g., *Gratier et al.*, 1999]. This distribution needs to be accounted for, at least in a simple fashion, in the compactional law. Indeed, because relaxation times entering the compaction law are directly associated with the grain size distribution (equations (5) to (8)), a wide distribution of grain sizes implies a wide distribution of relaxation times. The inclusion of a realistic

RTD is especially important if the process is diffusion-limited because of the power law relationship relating the grain sizes and the relaxation times in that case (equations (5) and (7)).

[12] In the study of the electrical properties of saturated porous rocks, it is customary to represent broad distributions of relaxation times in the induced polarization of saturated rocks and soils with the so-called "Cole-Cole" distribution [see *Cole and Cole*, 1941; *Taherian et al.*, 1990]. The Cole-Cole distribution is characterized by a single coefficient, c, that accounts for the broadness of the distribution of relaxation times and therefore of the broadness of the distribution of the grain sizes [see *Chelidze et al.*, 1977; *Pelton et al.*, 1978; *Chelidze and Gueguen*, 1999; *Kemna*, 2000].

[13] Under the assumption that the distribution of relaxation times is represented by a Cole-Cole distribution, the compressibility of our rheological model becomes

$$\beta(t) \equiv \beta F(t/\tau_0; c), \tag{9}$$

$$F(t/\tau_0; c) \equiv 1 - \sum_{n=0}^{\infty} \frac{(-1)^n \left(\frac{t}{\tau_0}\right)^{nc}}{\Gamma(1 + nc)}, \tag{10}$$

$$F(t/\tau_0; c) \equiv \sum_{n=1}^{\infty} \frac{(-1)^{n+1} \left(\frac{t}{\tau_0}\right)^{nc}}{\Gamma(1 + nc)}, \tag{11}$$

where $\Gamma(\ )$ is the gamma function defined by

$$\Gamma(x) = \int_0^\infty u^{x-1} e^{-u} du \tag{12}$$

($x > 0$). Note that the series development involved in equation (11) converges very slowly for $t/\tau_0 > 10$ and $c < 1$; thus a significant number of terms is required for a good convergence of the series. In the case $c = 1$, we recover the Debye distribution

$$F(t/\tau_0; 1) \equiv \sum_{n=1}^{\infty} \frac{(-1)^{n+1} \left(\frac{t}{\tau_0}\right)^n}{\Gamma(1 + n)}, \tag{13}$$

$$F(t/\tau_0; 1) \equiv 1 - \sum_{n=0}^{\infty} \frac{(-1)^n \left(\frac{t}{\tau_0}\right)^n}{\Gamma(1 + n)}, \tag{14}$$

$$F\left(\frac{t}{\tau_0}; 1\right) \equiv 1 - \sum_{n=0}^{\infty} \frac{\left(-\frac{t}{\tau_0}\right)^n}{n!} = 1 - \exp\left(-\frac{t}{\tau_0}\right), \tag{15}$$

as required for the internal consistency of the model. The RTD is given with the probability [*Cole and Cole*, 1941]

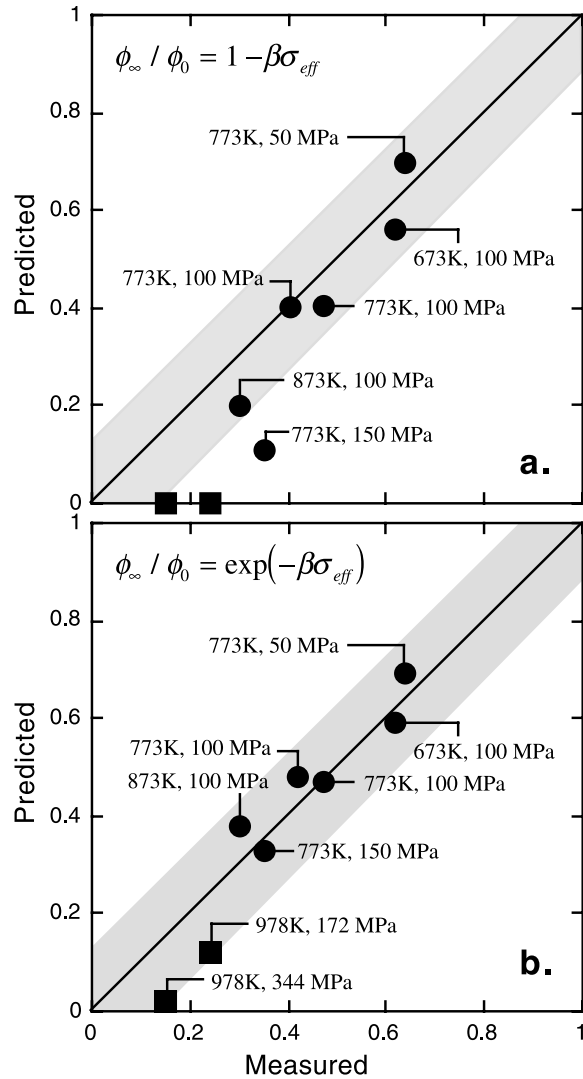$$P(s) = \left(\frac{1}{2\pi}\right) \frac{\sin[(1-c)\pi]}{\cosh(cs) - \cos[(1-c)\pi]}, \tag{16}$$

Figure 4. Comparison of the model predictions and laboratory experiments for the long-term compactional response ϕ_∞/ϕ_0 of porous aggregates. (a) Test of the linear relationship is shown. Note the discrepancy between the data and the model at high effective stresses. (b) Test of the exponential relationship is shown. The experiments cover a broad range of temperatures (400 to 700°C) and effective stresses (50 to 344 MPa) (solid circles, *Niemeijer et al.* [2002]; solid squares, *Lockner and Evans* [1995]). The final porosity is independent of the mean grain size. Indeed, the samples cover a broad mean grain size spectrum (from 5 to 85 μm). The gray bands represent uncertainty in determination of the porosity ratio.

where $s \equiv \ln(\tau/\tau_0)$, τ describes the distribution of relaxation times and τ_0 describes the peak of relaxation times given in section 2.1. The peak of the RTD is associated with the peak d_0 of the grain size distribution and c characterizes the broadness of the distribution. The probability distribution $P(s)$ has the property

$$\int_{-\infty}^{+\infty} P(s)\,ds = 1. \tag{17}$$

The Cole-Cole equation produces a very broad distribution of relaxation times when c is small (see Figure 2). For example for $c = 0.25$, 72 percent of the relaxation times are included in the range $10^{-3} < \tau/\tau_0 < 10^3$. When c is in the range $0.5-1$, the Cole-Cole distribution is quite similar to a log normal distribution. However, the Cole-Cole distribution has a longer tail than the log normal distribution when c is less than 0.5. The parameter c introduced in our model is not just a curve fitting parameter. It corresponds directly to the standard deviation of the logarithm of the grain size distribution assuming a log normal distribution. According to the dependence between relaxation times and the grain size (equations (5), (7), and (8)), the RTD can be compared directly with the particle size distribution (PSD).

[14] Some granular aggregates may exhibit RTDs that are not described by the Cole-Cole distribution. In these cases, other types of distribution can be considered in our model. For example, the Cole-Davidson distribution [*Davidson and Cole*, 1951] can account for nonsymmetrical PSD distributions of sediments or fault gouge. Using the properties of the convolution product, any distribution can be considered corresponding to a given grain size distribution. However, the mathematics are likely to become complex, and we will treat this elsewhere. In the present model, we show that the log normal PSD is a good approximation and therefore justifies the use of the Cole-Cole distribution.

3. Deviation From the Linear Model

[15] We now adapt the model of *Revil* [1999] to a wide range of effective stresses. At high effective stresses (typically ≥ 100 MPa), the experimental data by *Niemeijer et al.* [2002] show a clear departure from the linear model proposed in section 2. In the case of these experimental data, the effective stress history is simply

$$\sigma_{eff}(t) = \sigma_{eff}\mathrm{H}(t), \tag{18}$$

where H (t) is the Heaviside or step function (H (t) = 0 for $t < 0$ and H (t) = 1 for $t \geq 0$) and σ_{eff} is the imposed (constant) effective stress. Under this situation, the convolution integral in equation (1) yields the following linear compactional response

$$\phi(t) = \phi_0\left[1 - \beta(t)\sigma_{eff}\mathrm{H}(t)\right] \tag{19}$$

$$\phi(t) = \phi_0\left[1 - \beta\ F(t/\tau_0; c)\sigma_{eff}\mathrm{H}(t)\right]. \tag{20}$$

Table 2. Conditions of the Experiments of *Niemeijer et al.* [2002][a]

Run	T, °C	d, μm	σ_{eff}, MPa	ϕ_i[b]	ϕ_f[c]
Cpf3	500	47.1	100	0.2731	0.1271
Cpf4	500	42.9	150	0.2350	0.1051
Cpf5	500	40.5	50	0.2612	0.1660
Cpf6	400	40.9	100	0.2514	0.1536
Cpf7	600	43.2	100	0.3138	0.0970
Cpf8	500	11.7	100	0.3108	0.1465
Cpf9	500	85.9	100	0.2451	0.1032

[a]These experiments cover a wide range of effective stresses, temperatures, and mean grain size.
[b]Porosity at the beginning of the compaction process.
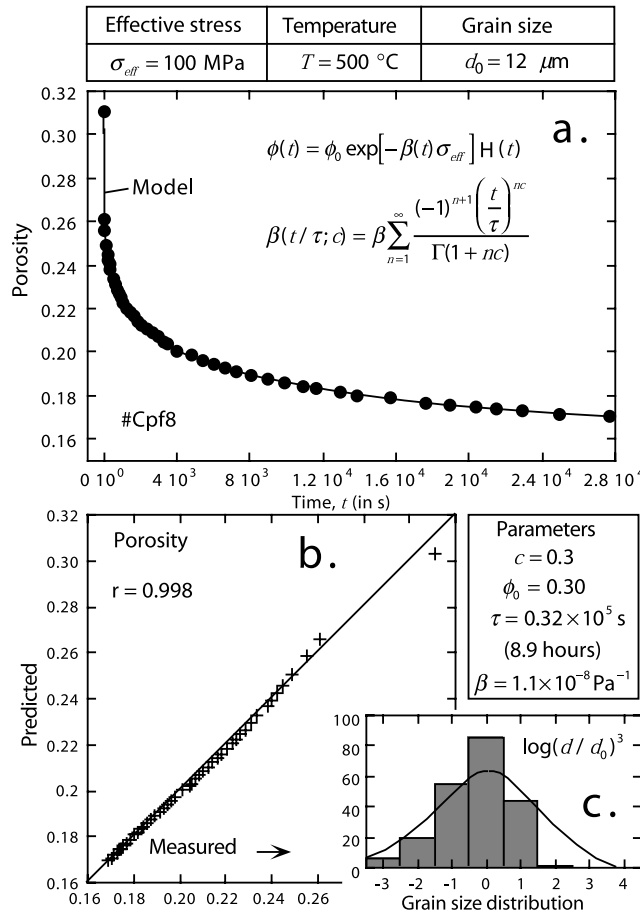[c]Porosity at the end of the compaction process.

Figure 5. (a) Compaction curve of a quartz aggregate in the initial stage of deformation. Data are from *Niemeijer et al.* [2002] (run Cpf8, effective pressure: 100 MPa, mean grain diameter: 12 μm, effective stress 100 MPa, temperature 500°C, $\phi_i = 0.311$). (b) Comparison between the predicted porosity and the measured porosity is shown. (c) Comparison between the measured grain size distribution and that predicted using the Cole-Cole distribution (plain line) is shown.

We show now that the previous equations can be modified to account for the observed nonlinear behavior of the compactional response at high effective stresses.

3.1. Long-Term Plastic Limit

[16] The long-term limit of the compactional response of the porous aggregate corresponds to timescales for which the duration of the experiment is much larger than the peak of the distribution of the relaxation times. When $t \gg \tau_0$, the compactional response reaches a linear "plastic" limit [*Stephenson et al.*, 1992]

$$\phi_\infty/\phi_0 = 1 - \beta\sigma_{eff}. \qquad (21)$$

The term "plastic" means that the compactional response is irreversible and that time does not appear explicitly in the constitutive rheological law. Equation (21) is valid under the assumption that $\beta\sigma_{eff} \ll 1$ [*Revil*, 2001] and a linearization of the compaction law can be performed. However, experiments performed at high effective stresses show unambiguously that

there is a deviation from linearity [see, e.g., *Niemeijer et al.*, 2002, Figure 2b]. We propose to correct this nonlinearity by replacing equation (21) with the plastic limit

$$\phi_\infty = \phi_0 \exp\left(-\beta\sigma_{eff}\right), \qquad (22)$$

which admits equation (21) as a limit when $\beta\sigma_{eff} \ll 1$, so for low effective stress levels ($\ll$100 MPa). Our choice of an exponential law is related to the exponential relationship between the solubility and the effective stress at the microscopic level.

[17] The first prediction of our model (prediction 1) is that the poroplastic limit is independent of the grain size distribution of the quartz sand. This prediction is in agreement with the experimental data of *Niemeijer et al.* [2002, Figure 2d]. Indeed for experiments performed with a wide range of mean grain sizes, in the range 12–86 μm (not to be misled with the grain size distribution of each sample), the compactional response ϕ_∞/ϕ_0 was observed for the narrow range 0.40–0.48. Figure 3b shows that the compaction coefficient is independent on the mean grain size of the porous aggregates.

[18] The dependence of the compaction coefficient on temperature is determined using an Arrhenius's law for β (Table 1) (prediction 2). Note that β is inversely proportional to the critical stress σ_c, which defines the limiting stress that grain-to-grain contacts can support without creeping [*Stephenson et al.*, 1992; *Revil*, 2001]. A similar behavior could exist for tectonic faults. We expect that the critical stress σ_c is temperature-dependent. *Revil* [1999] used a linear dependence between this critical stress and the temperature. The dependence of the compaction coefficient β on temperature can be also fitted with an Arrhenius law. This Arrhenius law is calibrated against the data of *Niemeijer et al.* [2002]. The final result is shown in Figure 3a and is reported in Table 1.

[19] A comparison between the long-term linear compaction law (equation (21)) and the exponential law (equation (22)) (Figure 4) shows that the exponential law provides a better description of the experimental data in the plastic limit of compaction. As these experimental data cover a broad range of temperatures (400 to 700°C) and effective stresses (50 to 344 MPa), the exponential model is likely to be more appropriate than the linear model.

3.2. Short-Term Compaction

[20] As for the long-term limit of compaction, we have to account for the nonlinear behavior discussed above for the

Table 3. Model Prediction of Experiments of *Niemeijer et al.* [2002]

Run	Θ_p,[a] Pa s^{-1}	Θ_d,[a] Pa s^{-1}	Θ_d,[a] Pa s^{-1}	Limited Process[b]	τ_0,[c] hours
Cpf3	6.70×10^{-14}	1.20×10^{-14}	1.02×10^{-14}	DL	145
Cpf4	7.36×10^{-14}	1.59×10^{-14}	1.31×10^{-14}	DL	113
Cpf5	7.79×10^{-14}	1.89×10^{-14}	1.52×10^{-14}	DL	97
Cpf6	17.0×10^{-14}	9.32×10^{-15}	6.02×10^{-15}	DL	174
Cpf7	2.31×10^{-13}	2.58×10^{-14}	2.32×10^{-14}	DL	83
Cpf8	2.70×10^{-13}	7.83×10^{-13}	2.01×10^{-13}	DPL	7.4
Cpf9	3.67×10^{-14}	1.98×10^{-15}	1.88×10^{-15}	DL	788

[a]Determined from equations (6), (7), and (8).
[b]DL, diffusion limited; DPL, dissolution/precipitation kinetics limited.
[c]Determined from equation (5) and Table 1.

Table 4. Results of Inversion for Experimental Data of *Niemeijer et al.* [2002][a]

Run	ϕ_0	c	β, $\times 10^{-8}$ Pa^{-1}
Cpf3	0.276 ± 0.002	0.35 ± 0.01	1.80 ± 0.02
Cpf4	0.245 ± 0.002	0.31 ± 0.01	2.45 ± 0.01
Cpf5	0.266 ± 0.002	0.34 ± 0.01	1.95 ± 0.03
Cpf6	0.262 ± 0.002	0.28 ± 0.01	1.17 ± 0.03
Cpf7	0.313 ± 0.002	0.31 ± 0.01	2.45 ± 0.13
Cpf8	0.308 ± 0.004	0.29 ± 0.01	1.07 ± 0.04
Cpf9	0.256 ± 0.002	0.30 ± 0.01	2.53 ± 0.04

[a]The reported values are the mean and twice the standard deviation of the a posteriori distributions of the model parameters.

full compactional response following the application of the stress. Indeed, very high values for the effective stresses were used in the experiments described by *Lockner and Evans* [1995] and *Niemeijer et al.* [2002]. Therefore we replace equation (19) by

$$\phi(t) = \phi_0 \exp\left[-\beta(t)\sigma_{eff}\right]\mathrm{H}(t), \qquad (23)$$

for $t > 0$. equation (23) admits equation (19) in the limit $\beta\sigma_{eff} \ll 1$.

4. Comparison With Experimental Results

[21] We use all the experimental data by *Niemeijer et al.* [2002] to test the compaction model developed above. Seven experiments were reported by *Niemeijer et al.* [2002] at various conditions of temperature, mean grain size, and effective pressure typical of the crust of the Earth. These conditions are reported in Table 2. *Niemeijer et al.* [2002] point out that an abrupt change in strain rate occurred, in all runs, after a few hours to ∼12 hours. They argue that this could be due to the fact that dissolved copper strongly hinders the dissolution rate of quartz and infiltration of dissolved copper from the cell into the samples during these experiments may have slow down compaction. However, such contamination is difficult to explain because the flux of water is outward from the samples during their compaction. Diffusion is a too slow process at this timescale
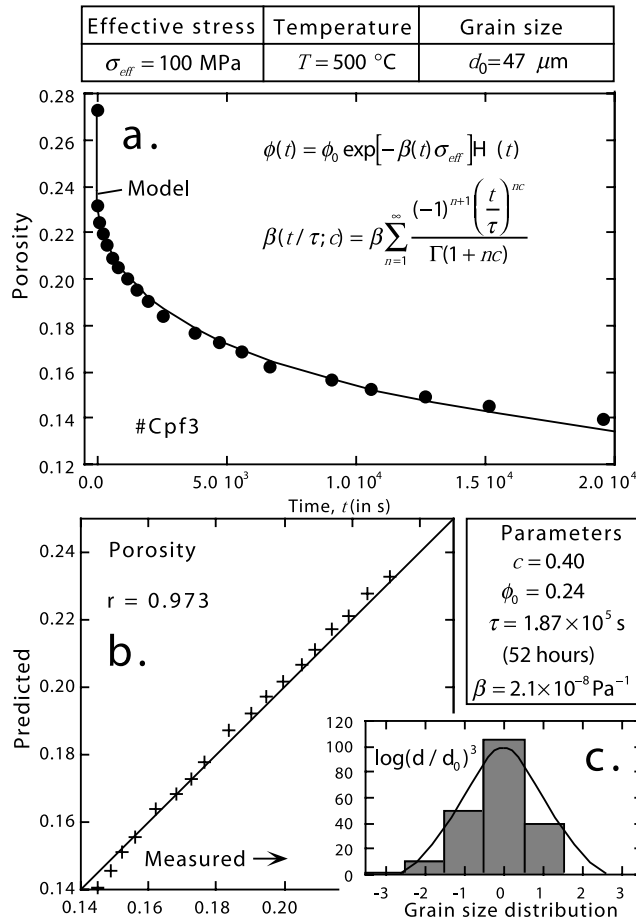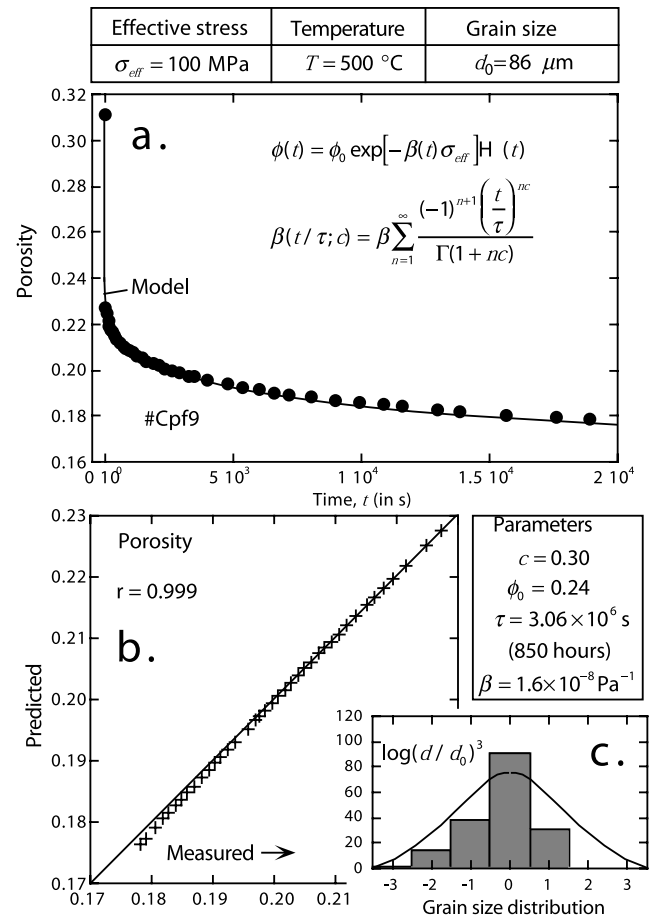

Figure 6. (a) Compaction curve of a quartz aggregate in the initial stage of deformation. Data are from *Niemeijer et al.* [2002] (run Cpf3, effective pressure 100 MPa, mean grain diameter 47 μm, effective stress 100 MPa, temperature 500°C, $\phi_i = 0.273$). (b) Comparison between the predicted and measured porosities is shown. (c) Comparison between the measured grain size distribution and that predicted using the Cole-Cole distribution (plain line) is shown.

Figure 7. (a) Compaction curve of a quartz aggregate in the initial stage of deformation. Data are from *Niemeijer et al.* [2002] (run Cpf9, effective pressure 100 MPa, mean grain diameter 86 μm, effective stress 100 MPa, temperature 500°C, $\phi_i = 0.24$). (b) Comparison between the predicted and measured porosities is shown. (c) Comparison between the measured grain size distribution and that predicted using the Cole-Cole distribution (plain line) is shown.
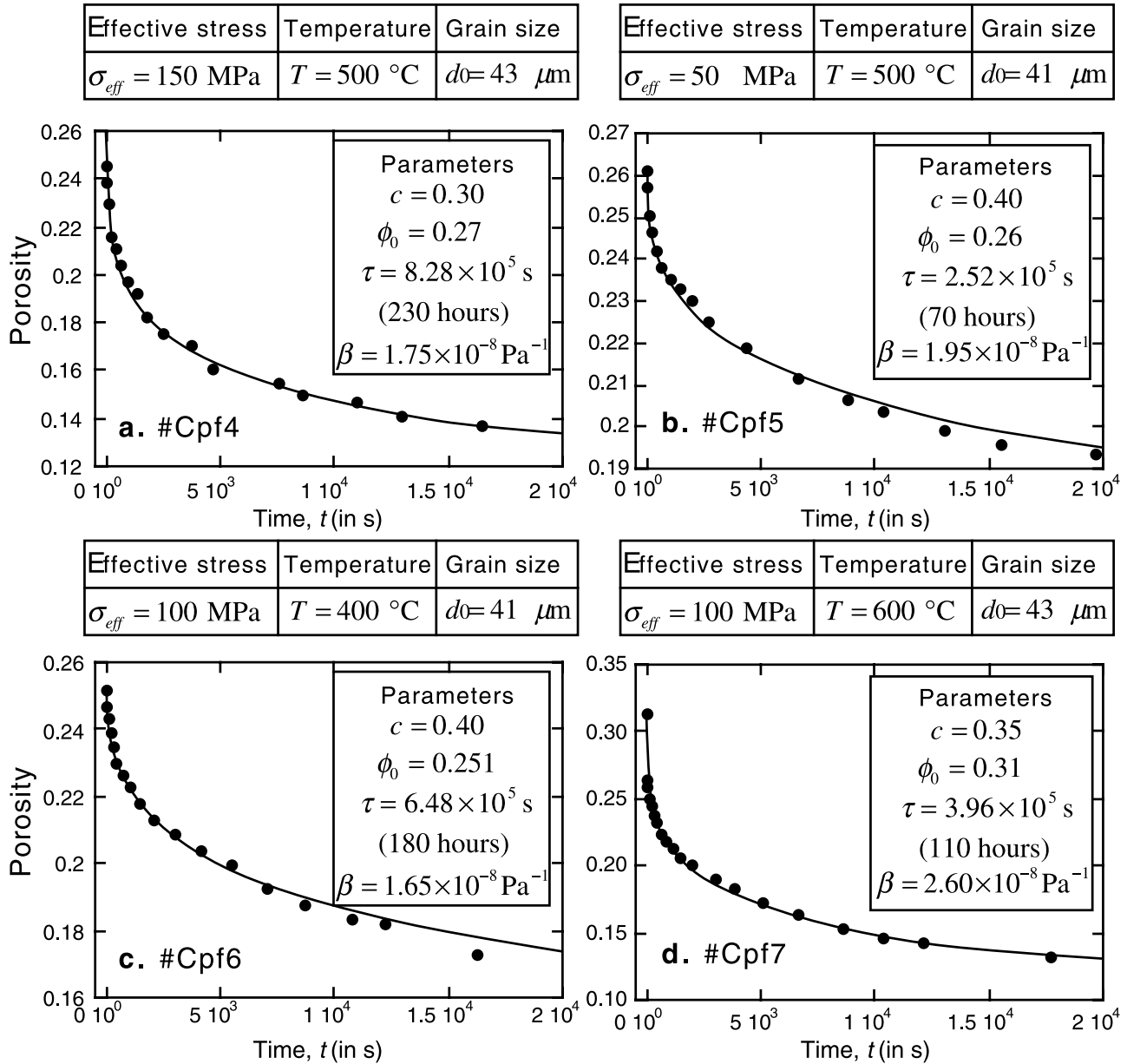
Effective stress	Temperature	Grain size
$\sigma_{eff} = 150$ MPa	$T = 500\ °C$	$do = 43\ \mu$m

Parameters
$c = 0.30$
$\phi_0 = 0.27$
$\tau = 8.28 \times 10^5$ s
(230 hours)
$\beta = 1.75 \times 10^{-8}$ Pa^{-1}

a. #Cpf4

Effective stress	Temperature	Grain size
$\sigma_{eff} = 50$ MPa	$T = 500\ °C$	$do = 41\ \mu$m

Parameters
$c = 0.40$
$\phi_0 = 0.26$
$\tau = 2.52 \times 10^5$ s
(70 hours)
$\beta = 1.95 \times 10^{-8}$ Pa^{-1}

b. #Cpf5

Effective stress	Temperature	Grain size
$\sigma_{eff} = 100$ MPa	$T = 400\ °C$	$do = 41\ \mu$m

Parameters
$c = 0.40$
$\phi_0 = 0.251$
$\tau = 6.48 \times 10^5$ s
(180 hours)
$\beta = 1.65 \times 10^{-8}$ Pa^{-1}

c. #Cpf6

Effective stress	Temperature	Grain size
$\sigma_{eff} = 100$ MPa	$T = 600\ °C$	$do = 43\ \mu$m

Parameters
$c = 0.35$
$\phi_0 = 0.31$
$\tau = 3.96 \times 10^5$ s
(110 hours)
$\beta = 2.60 \times 10^{-8}$ Pa^{-1}

d. #Cpf7

Figure 8. Compaction curves of quartz aggregates in the initial stage of deformation. Data are from *Niemeijer et al.* [2002]. The parameters given are fitted parameters, but their values are very close to independent evaluations from the equations developed in section 2.

over the length of the sample to allow copper to infiltrate through its pore network. As shown below, there is no need of such an hypothesis to explain the shape of the compaction curves.

[22] There are also some controversies regarding the relative roles of pressure solution versus cracking at grain-to-grain contacts. Cataclastic compaction by cracking that is fluid-assisted through reaction at the crack tip (and therefore thermally activated) can also be an important process of compaction, and the samples of *Niemeijer et al.* [2002] show abundant evidence of cracking. However, the high temperatures of the *Niemeijer et al.* [2002] experiments would tend to favor pressure solution as the dominant mechanism of deformation.

[23] For $t > 0$, the nonlinear compactional law is written explicitly as

$$\phi(t) = \phi_0 \exp\left[-\beta\sigma_{eff} \sum_{n=1}^{\infty} \frac{(-1)^{n+1}\left(\frac{t}{\tau_0}\right)^{nc}}{\Gamma(1 + nc)} \right]. \qquad (24)$$

[24] We first compare the prediction of this equation with the experimental data in the early stage of compaction (see Figures 5 to 8) using the fitting algorithm described in Appendix B. In Figure 9, we plot the mean relaxation times τ_0 determined by fitting equation (24) to the experimental data as a function of the relaxation times derived independently, in Table 3, using equations (6), (7), and (8). There is
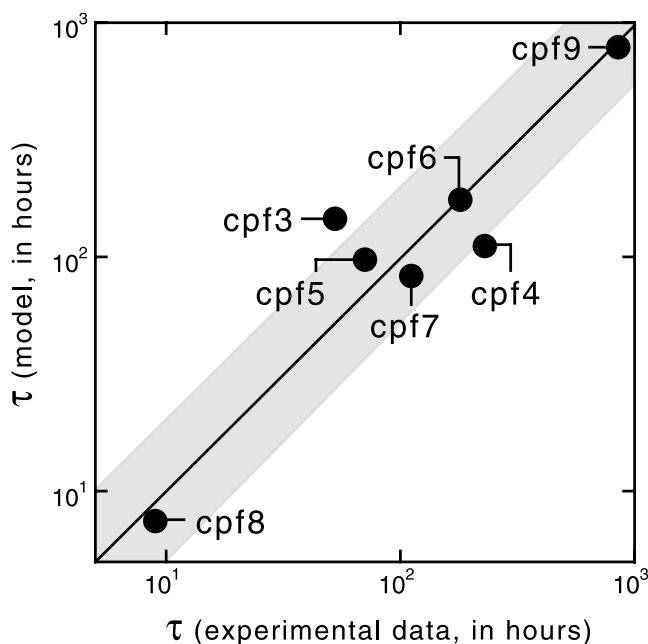
Figure 9. Comparison between the mean time τ_0 constant obtained by fitting the data to equation (24) (values reported in Figures 5 to 8) and the time constant determined independently from equations (5) to (8) and the values of parameters in the last column of Table 3. Cpfi corresponds to the experimental run "i". The grey band represents the uncertainty in determination of the mean relaxation time.

good agreement between the two estimates, so it follows that prediction 3 of the model is fine (the mean relaxation time of the viscoplastic model can be described (within a factor 2) using the mean grain diameter of the aggregate and temperature). Therefore, to diminish the number of fitting parameters when we consider all the experimental data, we use the value of the relaxation time τ_0 directly inferred from equations (6), (7), and (8).

[25] From the considerations given above, the parameters to invert are $\{\phi_0, \beta, c\}$. We use the inversion algorithm described in Appendix B. The results of the inversion, for the full set of the experimental data, are reported in Table 4. The fitted porosity ϕ_0 is very close to the initial porosity. This is expected from the small contribution of the poroelastic contribution (see demonstration in Appendix A). The compaction coefficient increases with temperature according to the Arrhenius law (Figure 3a) and the range of values of the compaction coefficient is consistent with that reported by *Revil* [2001]. The value of c implies a broad relaxation time distribution in agreement with the observed PSD (Figures 5, 6, 7, and 8) and the fact that the process is diffusion-limited. Indeed, as shown in Table 3, the kinetics of the compaction experiments are limited by the diffusion of the solute species at the grain-to-grain contacts. This implies that the relaxation time is an function of the grain size with a power law exponent equal to three, in agreement with available data (see Figures 5c, 6c, and 7c). So prediction 4 of the model, stated at the end of section 1, is also checked.

[26] All the parameters involved in our compaction model can be obtained independently. It follows that the only

factor that must be adjusted in our model is the Cole-Cole exponent. From the experiments made by *Niemeijer et al.* [2002], the Cole-Cole exponent falls in a narrow range $c = 0.30 \pm 0.05$. It follows that this range of values is recommended to model pervasive pressure solution transfer in such materials. Additional experiments would be useful to test whether the parameter value $c = 0.30$ is universal. If so, our model has no free parameters. The compaction model with $c = 0.30$ and experimental data are compared in Figure 9 and Figure 10. The agreement between the model and the experimental data provides a test of prediction 5: the same compactional model can be used to explain the full range of data obtained by *Niemeijer et al.* [2002] including the short-term viscous behavior and the long-term plastic limit.

[27] If the grain size distribution evolves during compaction, this implies that the value of c (that reflects the standard deviation of the lognormal distribution of the PSD) changes during the compaction. For example, if the grain size distribution appears more restricted at the end of the experiments than at the start of a run, this implies that the value of c increases during the experiment. Inversion for c, at different time steps, during compaction may be used to monitor the evolution of particle size distribution with time. This could be important for permeability modeling, for example, during fault zone healing (T. Dewers, personal communication, 2005).

5. Concluding Statements

[28] The model of *Revil* [1999] is modified using a Cole-Cole distribution of relaxation times and nonlinear compactional law at high effective stresses. The Cole-Cole
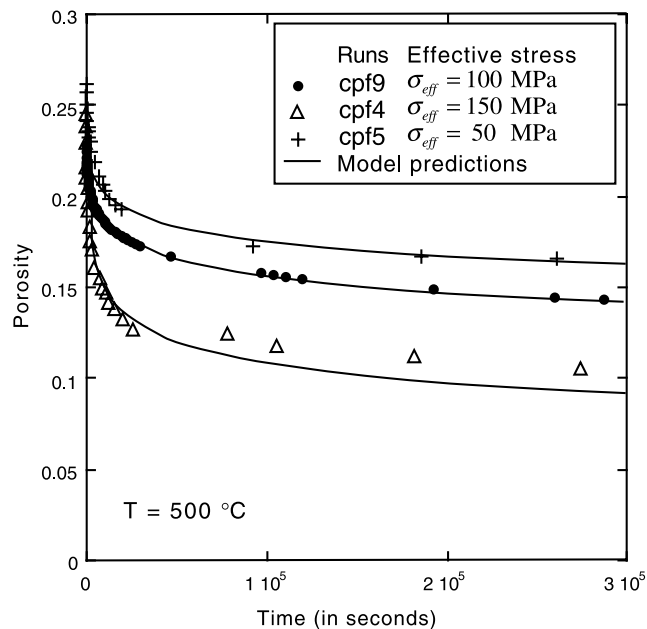

Figure 10. Test of the model for the effective stress. The compaction model is compared to compaction curves of three quartz aggregates, at the same temperature, but at different effective stresses ($c = 0.30$ and all the other parameters are determined from the equations developed in the main text and Table 1). Experimental data are from *Niemeijer et al.* [2002].

distribution is characterized by a single exponent c, which accounts for the distribution of the relaxation times. The case $c = 1$ corresponds to a Dirac distribution, which is in turn associated with a very sharp distribution of grain size (e.g., a Gaussian distribution with a very small variance). The use of a Cole-Cole response is intended to account for large grain size distributions in the compactional response of the porous aggregates. This modified model is compared to the experimental data obtained by *Niemeijer et al.* [2002] for which the grain size distributions cover more than 2 orders of magnitude, resulting in part from cataclasis in the early stage of deformation. We find a good agreement between the prediction of the model and the experimental data with $c = 0.30 \pm 0.05$. Because the kinetics of compaction are limited by diffusion (see Table 3), we expect that the RTD covers 5–6 orders of magnitude. This is in agreement with the previous value for the Cole-Cole exponent. Broad distributions of grain size likely exist during natural compaction and deformation of fault gouge.

[29] This new model has important implications for the dynamics of faults, the compactional response of sandstones in sedimentary basins, and subsidence related to changes of the effective stress in clastic oil/gas reservoirs. The model yields different predictions for the compactional response of porous aggregates from those using other rheologies (e.g., viscous or poroelastic). This model has also some applications to the study of solitary waves in the crust of the Earth [see *Revil and Cathles*, 2002; *Revil et al.*, 2003].

Appendix A: Poroelastic Contribution

[30] The total porosity change of the porous aggregate is written as

$$\frac{\partial \phi(t)}{\partial t} = \left(\frac{\partial \phi}{\partial t}\right)_e + \left(\frac{\partial \phi}{\partial t}\right)_i, \tag{A1}$$

where the first term of the right-hand side of equation (A1) (subscript e) corresponds to the poroelastic contribution and the second term of the right-hand side of equation (A1) (subscript i) corresponds to the (irreversible) compactional response associated with pressure solution. In Biot's theory, the poroelastic contribution to deformation is given by

$$\left(\frac{\partial \phi(t)}{\partial t}\right)_e = -\beta_e \left(\frac{\partial \sigma}{\partial t} - \alpha \frac{\partial p}{\partial t}\right), \tag{A2}$$

where ϕ is the porosity, σ is the confining pressure, and p is the pore fluid pressure. The elastic porosity compressibility β_e and the porosity effective stress coefficient α are defined by

$$\beta_e = \frac{1}{B}\left(\frac{1}{K} - \frac{1}{K_u}\right) - \frac{\phi}{K} \tag{A3}$$

$$\alpha = \frac{\phi/K_f + (\phi - 1/B)(1/K - 1/K_u)/B}{\phi/K - (1/K - 1/K_u)/B}, \tag{A4}$$

where B is the Skempton's coefficient, K is the drained bulk modulus, K_u is the undrained bulk modulus, and K_f is the

bulk modulus of the pore water. A simple analysis of the poroelastic compactional response indicates that it is much smaller than the PPST response in the experiments by *Niemeijer et al.* [2002]. Typically, $(\delta\phi/\phi)_e < 5\%$.

Appendix B: Fitting Procedure

[31] Equation (24) can be expressed as a nonlinear functional relationship of the form $\mathbf{d} = G(\mathbf{m})$ between the vector of model parameters $\mathbf{m}$ and the vector of porosity data $\mathbf{d}$:

$$\mathbf{d} = [\phi_1, \phi_2, \ldots, \phi_3]^T \tag{B1}$$

$$\mathbf{m} = [\phi_0, \beta, c]^T, \tag{B2}$$

where T signifies transpose. We use an a priori density probability corresponding to the null information in the range of possible values of the model parameters, which are $\phi_0 \in [0.20; 0.35]$, $\beta \in [0.5 \times 10^{-8}/\text{Pa}; 3.0 \times 10^{-8}/\text{Pa}]$, and $c \in [0; 1]$. The Simplex algorithm [*Caceci and Cacheris*, 1984] is used to minimize the least squares objective function

$$\min R = \| G(\mathbf{m}) - \mathbf{d}_0 \|^2, \tag{B3}$$

where $\|\mathbf{v}\| = (\mathbf{v}^T\mathbf{v})^{1/2}$ denotes the Euclidian (L_2) norm and $\mathbf{d}_o$ is the vector of the observed porosity data.

[32] We use an a priori model chosen randomly in the a priori set of values of the model parameters given above. Then, we determine the mean and the standard deviation of the optimized model parameters resulting from the use of the optimization process. Five hundred terms were considered in the series development involved in equation (24). The results are reported in Table 4.

References

Alcantar, N., J. Israelashvili, and J. Boles (2003), Forces and ionic transport between mica surfaces: implications for pressure solution, *Geochim. Cosmochim. Acta*, *67*, 1289–1304.

Caceci, M. S., and W. P. Cacheris (1984), Fitting curves to data, the Simplex algorithm is the answer, *Byte*, *9*, 340–362.

Chelidze, T. L., and Y. Gueguen (1999), Electrical spectroscopy of porous rocks: A review – I. Theoretical models, *Geophys. J. Int.*, *137*, 1–15.

Chelidze, T. L., A. I. Derevjanko, and O. D. Kurilenko (1977), *Electrical Spectroscopy of Heterogeneous Systems*, Naukova Dumka, Kiev, Russia.

Cole, K. S., and R. H. Cole (1941), Dispersion and adsorption in dielectrics. I. Alternating current characteristics, *J. Chem. Phys.*, *9*, 341–351.

Davidson, D. W., and R. H. Cole (1951), Dielectric relaxation in glycerol, propylene glycol, and n-propanol, *J. Chem. Phys.*, *29*, 1484–1490.

Dewers, T., and A. Hajash (1995), Rate laws for water assisted compaction and stress-induced water-rock interaction in sandstones, *J. Geophys. Res.*, *100*, 13,093–13,112.

Dewers, T., and P. Ortoleva (1990), A coupled reaction/transport/mechanical model for intergranular pressure solution stylolites, and differential

compaction and cementation in clean sandstones, *Geochim. Cosmochim. Acta*, *54*, 1609–1625.

Dove, P. M., and D. A. Crerar (1990), Kinetics of quartz dissolution in electrolyte solutions using a hydrothermal mixed flow reactor, *Geochim. Cosmochim. Acta*, *54*, 955–969.

Gratier, J.-P., F. Renard, and P. Labaume (1999), How pressure solution creep and fracturing processes interact in the upper crust to make it behave in both a brittle and viscous manner, *J. Struct. Geol.*, *21*, 1189–1197.

He, W., A. Hajash, and D. Sparks (2002), A model for porosity evolution during compaction of sediments, *Earth Planet. Sci. Lett.*, *197*, 237–244.

He, W., A. Hajash, and D. Sparks (2003), Creep compaction of quartz aggregates: Effect of pore fluid flow rates: A combined experimental and theoretical study, *Am. J. Sci.*, *303*, 73–93.

Iler, R. K. (1979), *The Chemistry of Silica*, John Wiley, Hoboken, N. J.

Ivins, E. R. (1996), Transient creep of a composite lower crust: 2. A polymineralic basis for rapidly evolving postseismic deformation modes, *J. Geophys. Res.*, *101*, 28,005–28,028.

Karner, S. L., F. M. Chester, A. K. Kronenberg, and J. S. Chester (2003), Subcritical compaction and yielding of granular quartz sand, *Tectonophysics*, *377*(3–4), 357–381.

Kemna, A. (2000), Tomographic inversion of complex resistivity: Theory and application, Ph.D. thesis, Bochum Univ., Osnabrück, Germany.

Leroy, P., A. Revil, and D. Coelho (2006), Diffusion of ionic species in bentonite, *J. Colloid Interface Sci.*, *296*, 248–255.

Lockner, D., and B. Evans (1995), Densification of quartz powder and reduction of conductivity at 700°C, *J. Geophys. Res.*, *100*, 13,081–13,092.

Montési, L. G. J. (2004), Controls of shear zone rheology and tectonic loading on postseismic creep, *J. Geophys. Res.*, *109*, B10404, doi:10.1029/2003JB002925.

Nakashima, S. (1995), Diffusivity of ions in pore water as a quantitative basis for rock deformation rate estimates, *Tectonophysics*, *245*, 185–203.

Niemeijer, A. R., and C. J. Spiers (2002), Compaction creep of quartz-muscovite mixtures at 500°C: Preliminary results on the influence of muscovite on pressure solution, in *Deformation Mechanisms, Rheology and Tectonics: Current Status and Future Perspectives*, edited by S. De Meer et al., London, *Geol. Soc. Spec. Publ.*, *200*, 61–71.

Niemeijer, A. R., C. J. Spiers, and B. Bos (2002), Compaction creep of quartz sand at 400–600°C: experimental evidence for dissolution-controlled pressure solution, *Earth Planet. Sci. Lett.*, *195*, 261–275.

Pelton, W. H., S. H. Ward, P. G. Hallof, W. R. Sill, and P. H. Nelson (1978), Mineral discrimination and removal of inductive coupling with multi-frequency IP, *Geophysics*, *43*, 588–609.

Renard, F., P. Ortoleva, and J. P. Gratier (1997), Pressure solution in sandstones: influence of clays and dependence on temperature and stress, *Tectonophysics*, *280*, 257–266.

Revil, A. (1999), Pervasive pressure-solution transfer: A poro-visco-plastic model, *Geophys. Res. Lett.*, *26*, 255–258.

Revil, A. (2001), Pervasive pressure solution transfer in a quartz sand, *J. Geophys. Res.*, *106*, 8665–8690.

Revil, A., and L. M. Cathles (2002), Fluid transport by solitary waves along growing faults: A field example from the South Eugene Island Basin, Gulf of Mexico, *Earth Planet. Sci. Lett.*, *202*, 321–335, (Erratum, *Earth Planet. Sci. Lett.*, *204*, 321–322, 2002).

Revil, A., D. Grauls, and O. Brévart (2002), Bulk mechanical compaction of sand shale mixtures, *J. Geophys. Res.*, *107*(B11), 2293, doi:10.1029/2001JB000318.

Revil, A., G. Saracco, and P. Labazuy (2003), The volcano-electric effect, *J. Geophys. Res.*, *108*(B5), 2251, doi:10.1029/2002JB001835.

Revil, A., P. Leroy, and K. Titov (2005), Characterization of transport properties of argillaceous sediments. Application to the Callovo-Oxfordian Argillite, *J. Geophys. Res.*, *110*, B06202, doi:10.1029/2004JB003442.

Rutter, E. H. (1976), The kinetics of rock deformation by pressure solution, *Philos. Trans., R. Soc. London, Ser. A*, *283*, 203–219.

Rutter, E. H. (1983), Pressure solution in nature, theory and experiment, *J. Geol. Soc. London*, *140*, 725–740.

Skvortsova, Z. N. (2004), Deformation by the mechanism of dissolution-reprecipitation as a form of adsorption plasticization of natural salts, *Colloid J.*, *66*(1), 1–10.

Stephenson, L. P., W. J. Plumley, and V. V. Palciauskas (1992), A model for sandstone compaction by grain interpenetration, *J. Sediment. Petrol.*, *62*, 11–22.

Taherian, M. R., W. E. Kenyon, and K. A. Safinya (1990), Measurement of dielectric response of water-saturated rocks, *Geophysics*, *55*(12), 1530–1541.

Wahab, A. A. (1998), Diagenetic history of Cambrian quartarenites, Ras Dib-Zeit bay area, Gulf of Suez, eastern desert, Egypt, *Sediment. Geol.*, *121*, 121–140.

Yang, X. S. (2000), Pressure solution in sedimentary basins: effect of temperature gradient, *Earth Planet. Sci. Lett.*, *176*, 233–243.

Yang, X. (2002), A mathematical model for voigt poro-visco-plastic deformation, *Geophys. Res. Lett.*, *29*(5), 1066, doi:10.1029/2001GL014014.

Yasuhara, H., D. Elsworth, and A. Polak (2003), A mechanistic model for compaction of granular aggregates moderated by pressure solution, *J. Geophys. Res.*, *108*(B11), 2530, doi:10.1029/2003JB002536.

Yasuhara, H., D. Elsworth, and A. Polak (2004), Evolution of permeability in a natural fracture: significant role of pressure solution, *J. Geophys. Res.*, *109*, B03204, doi:10.1029/2003JB002663.

Yasuhara, H., C. Marone, and D. Elsworth (2005), Fault zone restrengthening and frictional healing: The role of pressure solution, *J. Geophys. Res.*, *110*, B06310, doi:10.1029/2004JB003327.

————————————

A. Ghorbani and N. Florsch, University Paris VI, UMR 7619 "Sisyphe" Université Pierre et Marie Curie, Paris 6, Tour 56, 4 place Jussieu, F-75252 Paris Cedex 05, France.

P. Leroy and A. Revil, CNRS-CEREGE, BP 80, F-13545 Aix-en-Provence, Cedex 4, France. (leroy@cerege.fr; revil@cerege.fr)

A. R. Niemeijer, HPT Laboratory, Faculty of Geosciences, Utrech University, P.O. Box 80.021, NL-3508 TA Utrech, Netherlands. (niemeyer@geo.uu.nl)